CMS Physics Analysis Summary

Contact: cms-pag-conveners-heavyions@cern.ch 2017/02/07

Measurement of $\psi(2S)$ production in proton-lead and proton-proton collisions at $\sqrt{s_{NN}} = 5.02$ TeV

The CMS Collaboration

Abstract

This note reports the measurement of prompt ψ(2S) production in proton-lead (pPb) and proton-proton (pp) collisions at $\sqrt{s_{NN}} = 5.02$ TeV. The results are based on pPb and pp data samples collected by CMS at the LHC corresponding to an integrated luminosity of 34.6 nb^{-1} and 28.0 pb^{-1} respectively. The nuclear modification factor, R_{pPb}, is calculated for prompt ψ(2S) in the kinematic interval $4 < p_T < 30$ GeV/c and $-2.4 < y_{\mathrm{CM}} < 1.93$, and compared to the R_{pPb} of prompt J/ψ. The R_{pPb} of the excited state is found to be smaller than the R_{pPb} of the ground state, over the whole kinematic range studied. The suppression is more pronounced in the region of negative rapidity and $p_T < 10$ GeV/c.

1 Introduction

The interest of quarkonium physics in nuclear collisions has a long and rich history, which dates back to the original proposal by Matsui and Satz [1], predicting J/ψ suppression in heavy-ion collisions due to Debye screening in quark gluon plasma (QGP). Soon after the proposal, the first J/ψ measurements in heavy ion collisions were performed at the SPS, triggering an intense debate on the origin of the suppression reported experimentally [2, 3]. A similar amount of suppression has later been observed in AuAu collisions at RHIC at $\sqrt{s_{\mathrm{NN}}} = 200$ GeV [4, 5]. At the LHC, the production of charmonium (J/ψ, ψ(2S)) and bottomonium (Y(1S), Y(2S), Y(3S)) states has been studied in PbPb collisions at $\sqrt{s_{\mathrm{NN}}} = 2.76$ TeV and $\sqrt{s_{\mathrm{NN}}} = 5.02$ TeV [6–9], confirming the relevance of such analyses for the understanding of the medium produced in high-energy heavy ion collisions. The quarkonia yields are modified in the heavy ion collision due to quarkonia suppression inside QGP, regeneration from charm pairs and cold nuclear matter effects which has been demonstrated for J/ψ and Y in PbPb collisions [10]. An unambiguous interpretation of LHC results requires the quantitative understanding of cold nuclear matter effects. Among these effects, the nuclear parton distribution functions (nPDF) are known to differ from those in a free proton and thus impact the quarkonium yields in nuclear collisions [11, 12]. In addition, gluon radiation induced by parton multiple scattering in the nucleus leads to p_{T} broadening and coherent energy loss, resulting in a significant quarkonium suppression in nuclear collisions at all available energies [13, 14]. These phenomena are best studied in proton-nucleus collisions, in which hot medium effects are likely to be negligible. At the LHC, the cross section of J/ψ mesons in pPb collisions at $\sqrt{s_{\mathrm{NN}}} = 5.02$ TeV has been measured by the ALICE [15, 16], ATLAS [17], CMS [18] and LHCb [19] collaborations. A significant suppression of the prompt J/ψ yield in pPb collisions has been observed at forward y (proton-going direction) and low p_{T}, while no strong nuclear effects are reported at backward y (Pb-going direction). Measurements of Y(1S) in pPb collisions at $\sqrt{s_{\mathrm{NN}}} = 5.02$ TeV have also been performed by the ALICE [20] and LHCb [21], indicating less suppression than in the J/ψ channel.

Another piece of information is given by the behavior of the excited states, which are less tightly bound than the ground states and might suffer stronger suppression in proton-nucleus collisions. In the charmonium sector, ALICE [22] and LHCb [23] data showed that the suppression of ψ(2S), integrated over the transverse momentum, is more pronounced than that of the J/ψ. This observation may be compatible with the final state inelastic interaction of quarkonia in the medium produced in those collisions [24]. Regarding bottomonia, the double yield ratios Y(3S)/Y(1S) and Y(2S)/Y(1S) in pPb over pp collisions have been measured by CMS [25] and were found to be less than unity, indicating final state effects.

This note reports the analysis of ψ(2S) production in pp and pPb collisions at $\sqrt{s_{\mathrm{NN}}} = 5.02$ TeV collected with the CMS detector in 2013 (pPb sample) and in 2015 (pp sample). The measurements correspond to an integrated luminosity of (34.6 $\pm$ 1.2) nb^{-1} for pPb collisions and (28.0 $\pm$ 0.6) pb^{-1} for pp collisions. The ψ(2S) mesons are measured via their dimuon decay channel over $4 < p_{\mathrm{T}} < 30$ GeV/c and $-2.4 < y_{\mathrm{CM}} < 1.93$ in pp and pPb collisions. The ψ(2S) nuclear modification factor R_{pPb} is determined as a function of y_{CM} and p_{T} and compared to that of the J/ψ measured at the same center-of-mass energy.

2 CMS detector

A detailed description of the CMS detector and its components can be found in Ref. [26]. The detector consists of a superconducting solenoid with an internal diameter of 6 m, providing

a magnetic field of 3.8 T. Within the field volume are the silicon pixel and strip tracker, the crystal electromagnetic calorimeter, and the brass/scintillator hadronic calorimeter. The silicon pixel and strip tracker measure charged-particle trajectories in the range $|\eta| < 2.5$. It consists of 66 M pixel and 10 M strip sensor elements. Muons are detected in the range $|\eta| < 2.4$, with detection planes based on three technologies: drift tubes, cathode strip chambers, and resistive plate chambers. Because of the strong magnetic field and the fine granularity of the tracker, the muon p_{T} measurement based on information from the tracker alone has a resolution between 1 and 2% for typical muons in this analysis. The CMS apparatus also has extensive forward calorimetry, including two steel/quartz-fiber Čerenkov hadron forward calorimeters (HF), which cover $2.9 < |\eta| < 5.2$. These detectors are used for online event selection to reject background events from various sources.

3 Event selection

Proton lead collisions at center-of-mass energy per nucleon-nucleon pair $\sqrt{s_{\mathrm{NN}}} = 5.02$ TeV correspond to a proton beam of 4 TeV and a lead beam of 1.58 TeV per nucleon. The direction of the proton beam was set up to be clockwise in the first part of the run corresponding to 20.7 nb^{-1} and was reversed in the second part of the run. As a result of the beam energy difference, the nucleon-nucleon center-of-mass in pPb collisions is not at rest with respect to the laboratory frame. Massless particles emitted at $|\eta_{\mathrm{CM}}| = 0$ in the nucleon-nucleon center-of-mass frame are detected at $\eta_{\mathrm{lab}} = -0.465$ for the first run period (clockwise proton beam) and $+0.465$ for the second run period (counterclockwise proton beam) in the laboratory frame. In this note, forward regions (positive pseudorapidity) are defined by the direction of the proton beam. The pp dataset, collected at the same collision energy as pPb sample, corresponds to an integrated luminosity of 28.0 pb^{-1}. In this sample, ψ(2S) mesons are measured over $|y_{CM}| < 2.4$.

To remove beam related background, inelastic hadronic collisions are selected by requiring a coincidence of at least one of the HF calorimeter towers with more than 3 GeV of total energy in each side of the interaction point. Such selection is not required in pp collisions where the contribution of photon induced interactions is negligible compared to pPb. The pp and pPb events are further selected to have at least one reconstructed primary vertex composed of two or more associated tracks, within 25 cm from the nominal interaction point along the beam axis and within 2 cm in its transverse plane. To reject beam-scraping events, the fraction of good-quality tracks associated to the primary vertex is required to be larger than 25% when there are more than 10 tracks per event. In pPb collisions, an additional filter [27] is applied to remove multiple interactions per bunch crossing (pileup). After the selection, the residual fraction of pileup events is reduced from 3% to less than 0.2%.

The results presented here are based on dimuon events selected by the Level-1 (L1) trigger, a hardware-based trigger system requiring two muon candidates in the muon detectors with an inherent CMS detector acceptance $|y| \leq 2.4$. During offline analysis, muons are required to be within the following kinematic regions, which ensures single-muon reconstruction efficiencies above 10%:

$$\begin{aligned} |\eta^{\mu}| < 1.2 \quad &\rightarrow \quad p_T^{\mu} \geq 3.3 \text{ GeV}/c \\ 1.2 < |\eta^{\mu}| < 2.1 \quad &\rightarrow \quad p^{\mu} \geq (3.93 - 1.11|\eta^{\mu}|) \text{ GeV}/c \\ 2.1 < |\eta^{\mu}| < 2.4 \quad &\rightarrow \quad p_T^{\mu} > 1.3 \text{ GeV}/c \end{aligned} \tag{1}$$

The oppositely charged muon pairs are selected to originate from a common vertex with a χ^2

probability greater than 1%, and with standard identification criteria [27].

4 Yield extraction

The signal extraction procedure is similar to those in previous CMS analyses [28, 29]. The analysis was performed in parallel for J/ψ and ψ(2S). The J/ψ results are cross checked with the results of [18] to validate analysis methods and final ψ(2S) results are reported in this note. The dimuon mass distribution is fitted with signal and background contributions which describe both the J/ψ and ψ(2S) resonances. The unbinned maximum likelihood fitting technique, as implemented in the RooFit package [30], is used for yield extraction. The ψ(2S) yield was extracted from a common fit to the J/ψ and ψ(2S) peaks composed by the weighted sum of a Crystal Ball and a Gaussian functions. The Crystal Ball function $g_{\rm CB}(m)$ combines a Gaussian core and a power-law tail with an exponent n to account for energy loss due to final-state photon radiation, and a parameter α which defines the transition between the Gaussian and the power-law functions,

$$g_{\rm CB}(m) = \begin{cases} \frac{N}{\sqrt{2\pi}\,\sigma_{\rm CB}} \exp\left(-\frac{(m-m_0)^2}{2\,\sigma_{\rm CB}^2}\right), & \text{for } \frac{m-m_0}{\sigma_{\rm CB}} > -\alpha; \\ \frac{N}{\sqrt{2\pi}\,\sigma_{\rm CB}} \left(\frac{n}{|\alpha|}\right)^n \exp\left(-\frac{|\alpha|^2}{2}\right) \left(\frac{n}{|\alpha|} - |\alpha| - \frac{m-m_0}{\sigma_{\rm CB}}\right)^{-n}, & \text{for } \frac{m-m_0}{\sigma_{\rm CB}} \leq -\alpha. \end{cases} \tag{2}$$

The Crystal Ball and Gaussian functions have independent widths to accommodate the rapidity dependent dimuon invariant-mass resolution, but share a common mean. Same signal shapes are used for ψ(2S) and J/ψ fits in data with common α and n parameters. Mean and sigma of ψ(2S) are obtained from the fitted mean and sigma of J/ψ scaled with their PDG mass ratios ($m_{\psi(2S)}/m_{J/\psi}$ = 1.1902) [31]. During the fit, the following parameters are left free: m_0 (the J/ψ mass), $\sigma_{\rm CB}$, $N_{J/\psi}$ (the J/ψ yield), and $N_{\psi(2S)}$ (the ψ(2S) yield). The weight of the component of the Gaussian f is left free in the range [0, 0.5]. Guided by MC studies the value of parameter n is fixed at n =2.1 and the parameter α is left free in the range [1,3] to cover the different shapes in each of the $p_{\rm T}$ and rapidity bins. The underlying background is described by the Chebyshev polynomial of degree N. The degrees of the Chebychev polynomial describing the background shape is obtained in each bin of the analysis using a Negative Log-Likelihood (NLL) test. Several alternative fitting procedures have been tested and and the variations with respect to the nominal result are included in the systematic uncertainty computation as explained in Sec. 6.

The J/ψ and ψ(2S) mesons coming from b-hadron decays are called non-prompt charmonia. These non-prompt charmonia are identified using the secondary $\mu^+\mu^-$ vertex displaced from the primary collision vertex. The secondary $\mu^+\mu^-$ vertex is determined by pseudo-proper decay length expressed as

$$\ell^{2D}_{J/\psi} = L_{xy} \cdot m/p_{\rm T}, \tag{3}$$

where L_{xy} is the most probable b-hadron decay length in the laboratory frame and m is the PDG J/ψ mass, assumed for all dimuon pairs [32, 33]. The non-prompt charmonina are removed by requiring $\ell^{2D}_{J/\psi}$ to be smaller than a certain value [29], which is optimized using MC simulations in order to keep 90% of the prompt charmonia. The yields of prompt charmonia are calculated using the number of events passing and failing the $\ell^{2D}_{J/\psi}$ cut a method which involves using the prompt and non-prompt efficiencies of $\ell^{2D}_{J/\psi}$ cut obtained from simulation [29].

Figure 1 shows the fit of the dimuon mass distribution both to the J/ψ and ψ(2S) peaks, for some particular bins in dimuon $p_{\rm T}$ and rapidity in pPb data. The signal is fitted with Crystal Ball and Gaussian functions and background is described with Chebyshev polynomial.

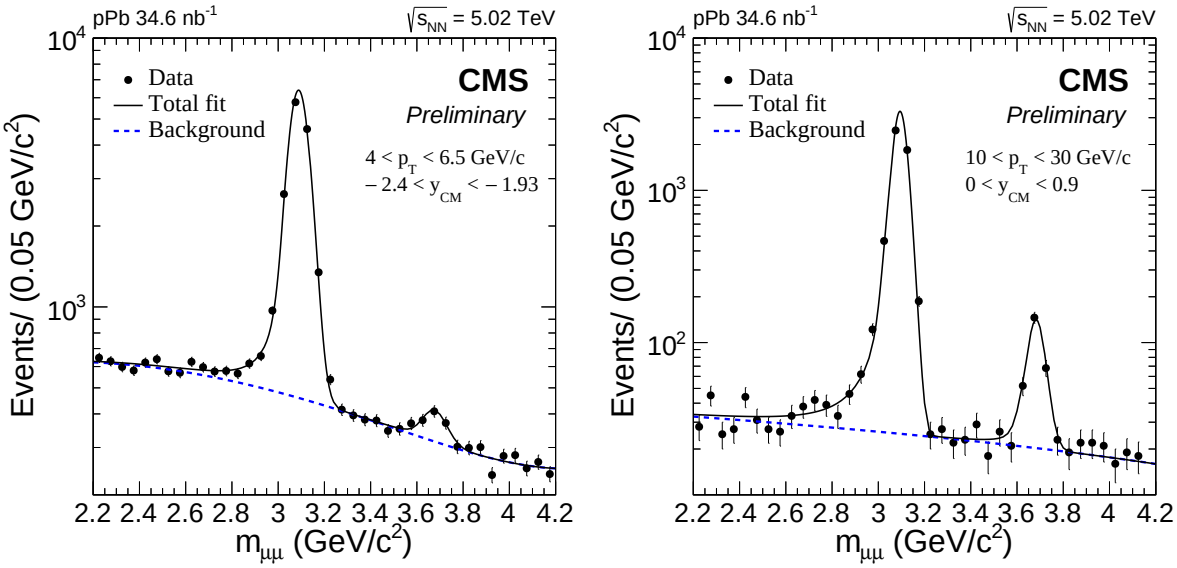

Figure 1: (Left) Fit of the dimuon mass distribution both to the J/ψ and ψ(2S) peaks of the pPb data in the kinematical bin $-2.4 < y_{\mathrm{CM}} < -1.93$ and $4 < p_{\mathrm{T}} < 6.5\,\mathrm{GeV}/c$. The signal is fitted with Crystal Ball and Gaussian functions and background is described with a Chebyshev polynomial of degree 3. (Right) Fit of the dimuon mass distribution both to the J/ψ and ψ(2S) peaks of the pPb data in the kinematical bin $0 < y_{\mathrm{CM}} < 0.9$ and $10 < p_{\mathrm{T}} < 30\,\mathrm{GeV}/c$. The signal is fitted with Crystal Ball and Gaussian functions and background is described with a Chebyshev polynomial of degree 3.

5 Acceptance and efficiency corrections

Monte Carlo (MC) events are used to obtain acceptance and efficiency correction factors to the measured J/ψ and ψ(2S) yields. Events are generated using PYTHIA version 6.4 [34] for pPb collisions and PYTHIA version 8.1 [35] for pp collisions. Generated particles in pPb simulation are boosted by $\Delta y = \pm 0.465$ to account for the asymmetry of proton and lead beams in the laboratory frame. In the absence of experimental information on quarkonium polarization in pPb and pp collisions at $\sqrt{s_{NN}}$ = 5.02 TeV, prompt J/ψ and ψ(2S) mesons are assumed to be produced unpolarized, as supported by the recent observations in pp collisions at $\sqrt{s}$ = 7 TeV [36]. The final-state QED radiation of the decay muons is taken into account using PHOTOS [37]. Finally the CMS detector response is simulated using GEANT 4 [38]. The J/ψ and ψ(2S) acceptance, is defined as the ratio of detectable muon pairs, dimuons passing the single muon selection cuts in eq. 1, to all generated charmonia in a given (p_{T}, y) bin. The reconstruction and trigger efficiency is obtained from MC and is defined as the ratio of number of reconstructed and triggered muon pairs to the number of generated and detectable muon pairs. The single muon efficiencies are obtained from data driven technique *tag-and-probe* (T&P), in a similar way as in Ref. [39]. The data-to-MC ratios of single muon efficiencies obtained from T&P, as a function of pseudorapidity and p_{T}, are applied to each of the two muons as scale factors to reweight, event-by-event, the number of reconstructed dimuons in the MC. The T&P correction factors are less than 5% for p_{T}^{μ} above 5 GeV/c. The largest T&P correction for the lowest $p_{\mathrm{T}}^{\mu\mu}$ bins, in the most forward and backward rapidities remains below 35% level. In addition, the deviations of the p_{T} spectrum in the MC samples from the data are taken into account by reweighing the dimuon events by the data/MC ratios as a function of p_{T} in each rapidity bin.

6 Systematic uncertainties

The systematic uncertainties arising from following sources are estimated: yield extraction method, T&P scaling factors, difference in the shape of data and MC p_T spectrum (p_T re-weighting) and from non-prompt rejection method. All these sources are explained in the following.

- **Signal Shape Variation** : The systematic uncertainty due to signal shape variation is obtained by changing the fitting constraints on the Crystal Ball (CB) parameters. For the nominal fitting, CB parameter n is fixed to the MC guided value (n=2.1) and the parameter α is restricted between 0.8 and 3 during fitting. In the first variation the yields are extracted by fixing the parameter α to the MC guided value (α=1.7) and n is left free in the range (1, 5). In the second variation, the yields of J/ψ and ψ(2S) are extracted by fixing both the parameters to their MC values $n = 2.1$, α=1.7. As both Crystal Ball parameters namely α and n are correlated to each other, the maximum of the absolute differences of the yields from the variations to the nominal yield is considered as error due to signal shape variation.
- **Background Shape Variation** : For the shape variation the degree of the polynomial is changed such that if the degree of polynomial is n for the nominal fitting, it is made $(n + 1)$ if n is 1 or 2 and $(n - 1)$ if n is 3. The absolute difference of the yield from this variation with respect to the nominal yield is the uncertainty due to background shape variation.
- **Uncertainty due to p_T shape in MC** : Since the acceptance and efficiency correction factors are affected by the kinematic variables, possible differences between MC and data are considered as source of a systematic uncertainty. The generated p_T distributions of MC samples are reweighted by the data/MC ratios for each rapidity bin. To obtain continuous reweighting factors, data/MC ratios are fitted with a linear function. We estimate the acceptance and efficiency values after reweighting the p_T and differences from nominal values are quoted as systematic uncertainties.
- **T&P scaling factors** : An uncertainty is assigned to account for the statistical uncertainty of the data sample on which the T&P scaling factors were calculated from, and for the systematic variations of the T&P method itself. The procedure is identical to the one used in [18].
- **Uncertainty due to non-prompt rejection method** : The full difference between the results with and without the non-prompt contamination correction is propagated as a systematic uncertainty due to non-prompt rejection method.

The systematic uncertainty due to yield extraction is determined by the uncertainties from the signal and background shape variations added in quadrature and lies between 2-25%. The systematic uncertainty due to corrections lies between 3-10%, which is obtained by adding in quadrature the uncertainty due to p_T shape in MC and the T&P uncertainty. The uncertainty due to non-prompt rejection method lies between 1-10%. The total systematic uncertainty is obtained by adding in quadrature the systematic uncertainties due to yield extraction, non-prompt rejection method and corrections and lies between 5-27%. An additiona global systematic uncertainty of 4.2% is applied due to integrated luminosity uncertainties of pp (2.3%) and pPb (3.5%) collisions.

7 Results

The nuclear modification factor (R_{pPb}) of ψ(2S) yields,

$$R_{\mathrm{pPb}}(p_{\mathrm{T}},y) = \frac{N_{\mathrm{pPb}}(p_{\mathrm{T}},y)}{A\,N_{\mathrm{pp}}(p_{\mathrm{T}},y)}\,\frac{\epsilon_{\mathrm{pp}}(p_{\mathrm{T}},y)}{\epsilon_{\mathrm{pPb}}(p_{\mathrm{T}},y)}\,\frac{\mathcal{A}_{\mathrm{pp}}(p_{\mathrm{T}},y)}{\mathcal{A}_{\mathrm{pPb}}(p_{\mathrm{T}},y)}\,\frac{\mathcal{L}_{\mathrm{pp}}}{\mathcal{L}_{\mathrm{pPb}}} \tag{4}$$

has been measured as a function of the charmonium transverse momentum and rapidity. In Eq. (4), $\mathcal{A}_{\mathrm{pp/pPb}}$ is the detector acceptance and $\epsilon_{\mathrm{pp/pPb}}$ is the reconstruction efficiency. The integrated luminosity values used are $\mathcal{L}_{\mathrm{pPb}} = 34.6\,\mathrm{nb}^{-1}$ for pPb collisions and $\mathcal{L}_{\mathrm{pp}} = 28.0\,\mathrm{pb}^{-1}$ is the integrated luminosity for pp collisions, and $A = 208$ is the Pb mass number.

Figure 2 shows the rapidity dependence of R_{pPb} for prompt ψ(2S) in three p_{T} ranges, $4.0 < p_{\mathrm{T}} < 6.5$ GeV/c (upper left), $6.5 < p_{\mathrm{T}} < 10$ GeV/c (upper right), and $10 < p_{\mathrm{T}} < 30$ GeV/c (bottom). The error bars represent the statistical uncertainties, and the boxes show the quadratic sum of systematic uncertainties. The fully correlated global uncertainty of 4.2% is displayed as a grey box around $R_{\mathrm{pPb}} = 1$. In both bins, $4.5 < p_{\mathrm{T}} < 6.5$ GeV/c and $6.5 < p_{\mathrm{T}} < 10$ GeV/c, the values of R_{pPb} prove below one independent of the rapidity, while in the largest p_{T} bin ($10 < p_{\mathrm{T}} < 30$ GeV/c) R_{pPb} is consistent with (yet systematically smaller than) unity. For comparison, the J/ψ nuclear modification factor [18] is also shown in Figure 2 as full squares symbols. Interestingly, the values of the J/ψ R_{pPb} lie systematically above those in the ψ(2S) channel, indicating different nuclear effects in the production of ground state and excited states.

Figure 3 shows the p_{T} dependence of R_{pPb} for prompt ψ(2S) in four rapidity bins. The error bars represent the statistical uncertainties, and the boxes show the quadratic sum of systematic uncertainties. The fully correlated global uncertainty of 4.2% is displayed as a grey box arround $R_{\mathrm{pPb}} = 1$. As can be seen in Figure 3, the values of R_{pPb} in the lowest p_{T} bins are significantly below unity in all rapidity bins.

The relative suppression of ψ(2S) compared to J/ψ observed in Figure 2 is reminiscent of what has been measured by the ALICE [22] and LHCb [23] collaboration on the p_{T}-integrated charmonium production in pPb collisions at the same collision energy. It is therefore interesting to note that such a difference subsists even at larger transverse momentum, although it seems to fade away in the largest p_{T} bin. While nPDF and coherent energy loss are the most discussed effects to explain J/ψ suppression [11–14], these two processes are expected to affect similarly the nuclear production ratio of J/ψ and ψ(2S) states, $R^{\mathrm{J}/\psi}_{\mathrm{pPb}} = R^{\psi(2\mathrm{S})}_{\mathrm{pPb}}$. On the contrary, the final state interaction of charmonia in the produced medium might lead to a stronger ψ(2S) suppression due to a larger inelastic cross section with comoving particles, as discussed in the model of Ref. [24] which as yet does not predict the p_{T} dependence of charmonium suppression. The present measurements at large transverse momentum ($4.5 < p_{\mathrm{T}} < 30$ GeV/c) and over a wide rapidity range ($-2.4 < y_{\mathrm{CM}} < 1.93$) should thus be able to bring stringent constraints and help elucidating the origin of quarkonium excited state suppression in pPb collisions at the LHC.

8 Summary

The pPb and pp collision data at $\sqrt{s_{\mathrm{NN}}} = 5.02$ TeV taken by the CMS detector are used to investigate the production of prompt ψ(2S). The results are based on pPb and pp data samples collected by CMS at the LHC corresponding to an integrated luminosity of 34.6 nb^{-1} and 28.0 pb^{-1} respectively. The nuclear modification factor of prompt ψ(2S) is determined in the kinematic interval $4 < \mathrm{p}_T < 30$ GeV/c and $-2.4 < \mathrm{y_{CM}} < 1.93$, and compared to the $\mathrm{R_{pPb}}$ of prompt J/ψ. The suppression is more pronounced in the region of negative rapidity and at

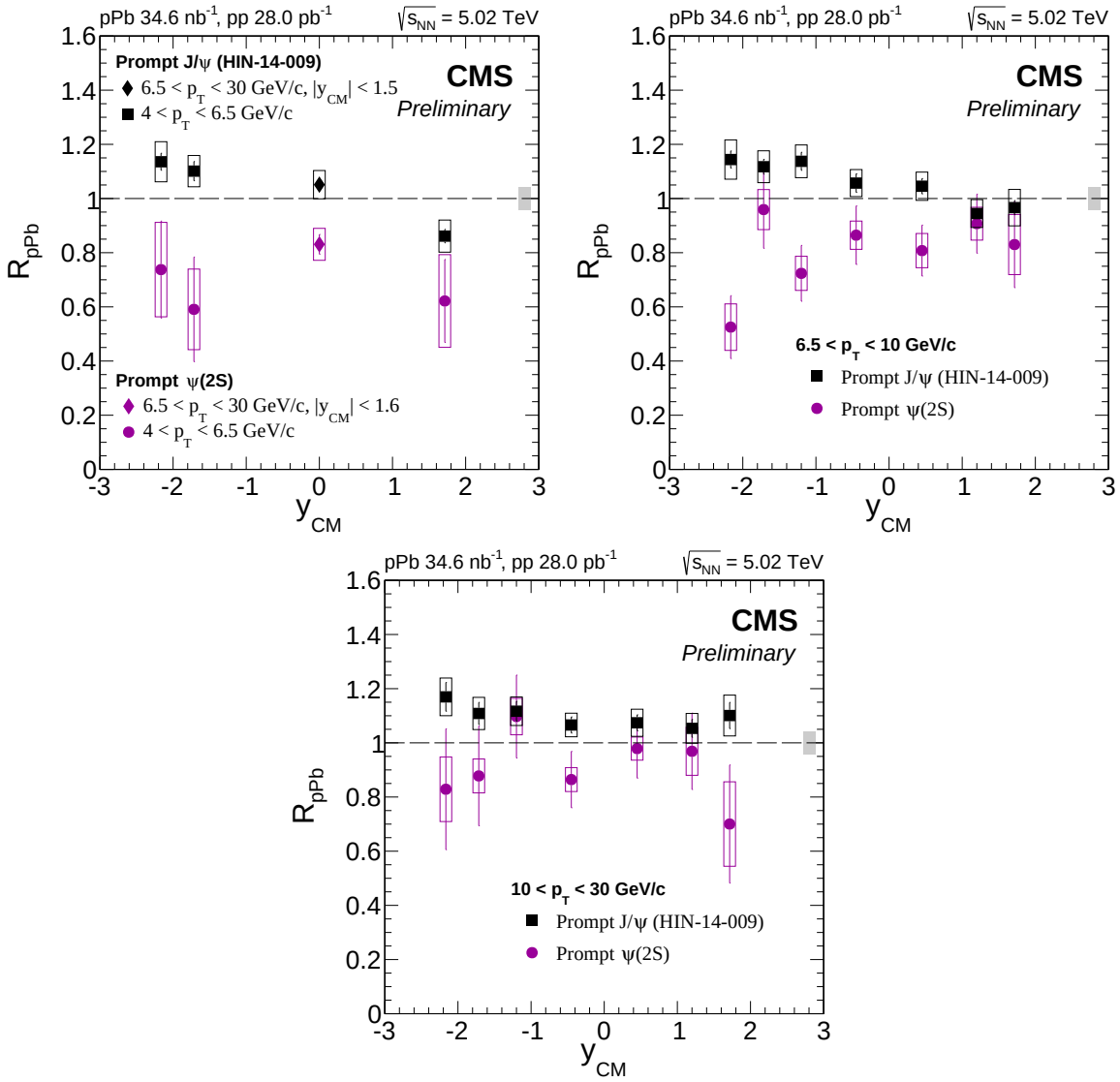

Figure 2: Rapidity dependence of R_{pPb} for prompt ψ(2S) in three p_{T} ranges. The error bars represent the statistical uncertainties, and the boxes show the quadratic sum of systematic uncertainties. The fully correlated global uncertainty of 4.2% is displayed as a grey box arround $R_{\mathrm{pPb}} = 1$.

$\mathrm{p}_T < 10$ GeV/c. The R_{pPb} of ψ(2S) is also found to be smaller to that of the J/ψ measured in Ref. [18], over the whole kinematic range studied. The different nuclear dependence of J/ψ and ψ(2S) reported here cannot be attributed to nPDF or coherent energy loss effects which predict a similar suppression in both channels. It may however be consistent with the picture of final state inelastic interaction of ψ(2S) mesons in the medium produced in pPb collisions at $\sqrt{s_{\mathrm{NN}}} = 5$ TeV.

References

[1] T. Matsui and H. Satz, "J/ψ Suppression by Quark-Gluon Plasma Formation", *Phys. Lett. B* **178** (1986) 416, doi:10.1016/0370-2693(86)91404-8.

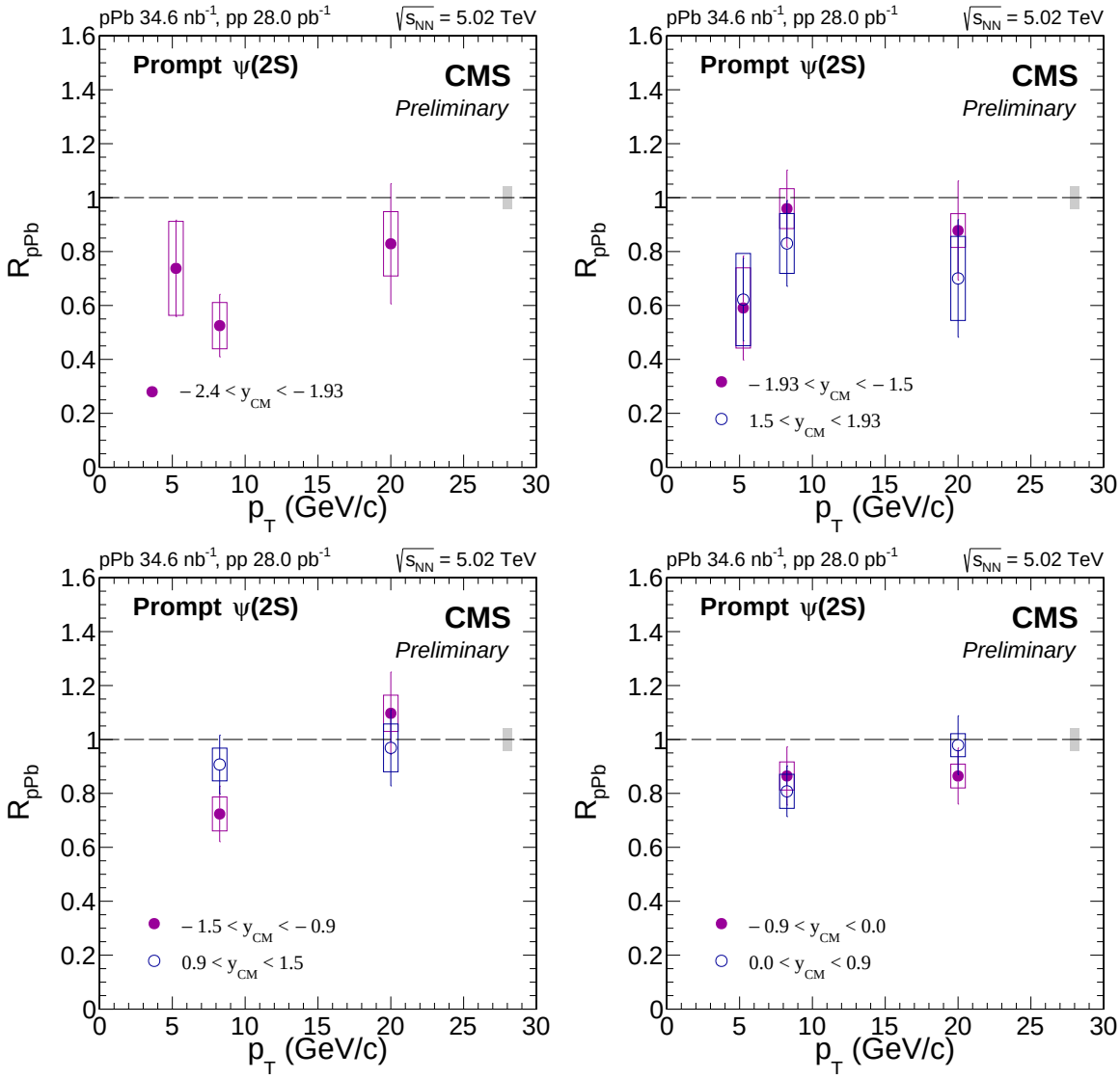

Figure 3: Transverse momentum p_T dependence of R_{pPb} for prompt ψ(2S) in four rapidity ranges. The error bars represent the statistical uncertainties, and the shaded boxes show the quadratic sum of systematic uncertainties. The fully correlated global uncertainty of 4.2% is displayed as a grey box arround $R_{pPb} = 1$.

[2] NA38 Collaboration, "The Production of J/ψ in 200-GeV/nucleon Oxygen Uranium Interactions", *Phys. Lett. B* **220** (1989) 471–478, doi:10.1016/0370-2693(89)90905-2.

[3] NA50 Collaboration, "Anomalous J / psi suppression in Pb - Pb interactions at 158 GeV/c per nucleon", *Phys. Lett. B* **410** (1997) 337–343, doi:10.1016/S0370-2693(97)00915-5.

[4] PHENIX Collaboration, "J/ψ production versus centrality, transverse momentum, and rapidity in AuAu collisions at $\sqrt{s_{NN}}$ = 200 GeV", *Phys. Rev. Lett.* **98** (2007) 232301, doi:10.1103/PhysRevLett.98.232301, arXiv:nucl-ex/0611020.

[5] PHENIX Collaboration, "J/ψ suppression at forward rapidity in Au+Au collisions at $\sqrt{s_{NN}}$ = 200 GeV", *Phys. Rev. C* **84** (2011) 054912,

doi:10.1103/PhysRevC.84.054912, arXiv:1103.6269.

[6] ALICE Collaboration, "Centrality, rapidity and transverse momentum dependence of J/ψ suppression in Pb-Pb collisions at $\sqrt{s_{\rm NN}}$=2.76 TeV", *Phys. Lett. B* **734** (2014) 314–327, doi:10.1016/j.physletb.2014.05.064, arXiv:1311.0214.

[7] CMS Collaboration, "Indications of suppression of excited Y states in PbPb collisions at $\sqrt{S_{NN}}$ = 2.76 TeV", *Phys. Rev. Lett.* **107** (2011) 052302, doi:10.1103/PhysRevLett.107.052302, arXiv:1105.4894.

[8] CMS Collaboration, "Observation of sequential Upsilon suppression in PbPb collisions", *Phys. Rev. Lett.* **109** (2012) 222301, doi:10.1103/PhysRevLett.109.222301, arXiv:1208.2826.

[9] CMS Collaboration, "Suppression of non-prompt J/ψ, prompt J/ψ, and Y(1S) in PbPb collisions at $\sqrt{s_{NN}} = 2.76$ TeV", *JHEP* **05** (2012) 063, doi:10.1007/JHEP05(2012)063, arXiv:1201.5069.

[10] V. Kumar, P. Shukla, and R. Vogt, "Quarkonia suppression in PbPb collisions at $\sqrt{s_{NN}}$ = 2.76 TeV", *Phys. Rev.* **C92** (2015), no. 2, 024908, doi:10.1103/PhysRevC.92.024908, arXiv:1410.3299.

[11] E. Ferreiro, F. Fleuret, J. Lansberg, and A. Rakotozafindrabe, "Impact of the Nuclear Modification of the Gluon Densities on J/ψ production in pPb collisions at $\sqrt{s_{\rm NN}}$ =5 TeV", *Phys. Rev. C* **88** (2013) 047901, doi:10.1103/PhysRevC.88.047901, arXiv:1305.4569.

[12] R. Vogt, "Shadowing effects on J/ψ and Y production at energies available at the CERN Large Hadron Collider", *Phys. Rev. C* **92** (2015) 034909, doi:10.1103/PhysRevC.92.034909, arXiv:1507.04418.

[13] F. Arleo and S. Peigné, "J/ψ suppression in p-A collisions from parton energy loss in cold QCD matter", *Phys. Rev. Lett.* **109** (2012) 122301, doi:10.1103/PhysRevLett.109.122301, arXiv:1204.4609.

[14] F. Arleo, R. Kolevatov, S. Peigné, and M. Rustamova, "Centrality and $p_\perp$ dependence of J/ψ suppression in proton-nucleus collisions from parton energy loss", *JHEP* **05** (2013) 155, doi:10.1007/JHEP05(2013)155, arXiv:1304.0901.

[15] ALICE Collaboration, "J/ψ production and nuclear effects in p-Pb collisions at $\sqrt{s_{\rm NN}} = 5.02$ TeV", *JHEP* **02** (2014) 073, doi:10.1007/JHEP02(2014)073, arXiv:1308.6726.

[16] ALICE Collaboration, "Rapidity and transverse-momentum dependence of the inclusive J/ψ nuclear modification factor in p-Pb collisions at $\sqrt{s_{\rm NN}} = 5.02$ TeV", *JHEP* **06** (2015) 055, doi:10.1007/JHEP06(2015)055, arXiv:1503.07179.

[17] ATLAS Collaboration, "Measurement of differential J/ψ production cross sections and forward-backward ratios in p+Pb collisions with the ATLAS detector", *Phys. Rev. C* **92** (2015) 034904, doi:10.1103/PhysRevC.92.034904, arXiv:1505.08141.

[18] CMS Collaboration, "J/ψ production in p Pb collisions", *To be submitted to EPJC* (2017).

[19] LHCb Collaboration, "Study of J/ψ production and cold nuclear matter effects in pPb collisions at $\sqrt{s_{\rm NN}}$ =5 TeV", *JHEP* **02** (2014) 072, doi:10.1007/JHEP02(2014)072, arXiv:1308.6729.

[20] ALICE Collaboration, "Production of inclusive Y(1S) and Y(2S) in p-Pb collisions at $\sqrt{\mathbf{s}_{\rm NN}} = \mathbf{5.02}$ TeV", *Phys. Lett. B* **740** (2015) 105–117, doi:10.1016/j.physletb.2014.11.041, arXiv:1410.2234.

[21] LHCb Collaboration, "Study of Y production and cold nuclear matter effects in pPb collisions at $\sqrt{s_{NN}}$=5 TeV", *JHEP* **07** (2014) 094, doi:10.1007/JHEP07(2014)094, arXiv:1405.5152.

[22] ALICE Collaboration, "Suppression of ψ(2S) production in p-Pb collisions at $\sqrt{s_{\rm NN}}$ = 5.02 TeV", *JHEP* **12** (2014) 073, doi:10.1007/JHEP12(2014)073, arXiv:1405.3796.

[23] LHCb Collaboration, "Study of $\psi(2S)$ production and cold nuclear matter effects in pPb collisions at $\sqrt{s_{NN}} = 5$ TeV", *JHEP* **03** (2016) 133, doi:10.1007/JHEP03(2016)133, arXiv:1601.07878.

[24] E. G. Ferreiro, "Excited charmonium suppression in protonnucleus collisions as a consequence of comovers", *Phys. Lett. B* **749** (2015) 98–103, doi:10.1016/j.physletb.2015.07.066, arXiv:1411.0549.

[25] CMS Collaboration, "Event activity dependence of Y(nS) production in $\sqrt{s_{NN}}$=5.02 TeV pPb and $\sqrt{s}$=2.76 TeV pp collisions", *JHEP* **04** (2014) 103, doi:10.1007/JHEP04(2014)103, arXiv:1312.6300.

[26] CMS Collaboration, "The CMS experiment at the CERN LHC", *JINST* **3** (2008) S08004, doi:10.1088/1748-0221/3/08/S08004.

[27] CMS Collaboration, "Performance of CMS muon reconstruction in pp collision events at $\sqrt{s} = 7$ TeV", *JINST* **7** (2012) P10002, doi:10.1088/1748-0221/7/10/P10002, arXiv:1206.4071.

[28] CMS Collaboration, "Measurement of Prompt ψ(2S) to J/ψ Yield Ratios in Pb-Pb and $p-p$ Collisions at $\sqrt{s_{NN}} = 2.76$TeV", *Phys. Rev. Lett.* **113** (2014), no. 26, 262301, doi:10.1103/PhysRevLett.113.262301, arXiv:1410.1804.

[29] CMS Collaboration, "Relative modification of prompt ψ(2S) and J/ψ yields from pp to PbPb collisions at $\sqrt{s_{\rm NN}} = 5.02$ TeV", *Submitted to: Phys. Rev. Lett.* (2016) arXiv:1611.01438.

[30] W. Verkerke and D. P. Kirkby, "The RooFit toolkit for data modeling", *eConf* **C0303241** (2003) MOLT007, arXiv:physics/0306116. [,186(2003)].

[31] Particle Data Group, J. Beringer et al., "Review of Particle Physics", *Phys. Rev. D* **86** (2012) 010001, doi:10.1103/PhysRevD.86.010001.

[32] ALEPH Collaboration, "Measurement of the $\overline{\rm B}^0$ and $\rm B^-$ meson lifetimes", *Phys. Lett. B* **307** (1993) 194, doi:10.1016/0370-2693(93)90211-Y.

[33] ALEPH Collaboration, "Errata: Measurement of the $\overline{\rm B}^0$ and $\rm B^-$ meson lifetimes", *Phys. Lett. B* **325** (1994) 537, doi:10.1016/0370-2693(94)90054-X.

[34] T. Sjöstrand, S. Mrenna, and P. Skands, "PYTHIA 6.4 physics and manual", *JHEP* **05** (2006) 026, doi:10.1088/1126-6708/2006/05/026, arXiv:hep-ph/0603175.

[35] T. Sjöstrand, S. Mrenna, and P. Skands, "A Brief Introduction to PYTHIA 8.1", *Comput. Phys. Commun.* **178** (2008) 852–867, doi:10.1016/j.cpc.2008.01.036, arXiv:0710.3820.

[36] CMS Collaboration, "Measurement of the prompt J/ψ and ψ(2S) polarizations in pp collisions at $\sqrt{s}$ = 7 TeV", *Phys. Lett. B* **727** (2013) 381, doi:10.1016/j.physletb.2013.10.055, arXiv:1307.6070.

[37] E. Barberio, B. van Eijk, and Z. Was, "PHOTOS: A Universal Monte Carlo for QED radiative corrections in decays", *Comput. Phys. Commun.* **66** (1991) 115–128, doi:10.1016/0010-4655(91)90012-A.

[38] GEANT4 Collaboration, "GEANT4: A Simulation toolkit", *Nucl. Instrum. Meth.* **A506** (2003) 250–303, doi:10.1016/S0168-9002(03)01368-8.

[39] CMS Collaboration, "Measurements of Inclusive W and Z Cross Sections in pp Collisions at $\sqrt{s} = 7$ TeV", *JHEP* **01** (2011) 080, doi:10.1007/JHEP01(2011)080, arXiv:1012.2466.